Journal of Atomic, Molecular, Condensate & Nano Physics
Vol. 2, No. 1, pp. 55–72, 2015
ISSN 2349-2716 (online); 2349-6088 (print)
Published by RGN Publications

http://www.rgnpublications.com

Free-free Transitions of the Hydrogenic Systems Inside a Dense Plasma Irradiated by a Laser Field

Research Article

A. K. Bhatia

Solar Physics Laboratory, NASA/Goddard Space Flight Center Greenbelt, Maryland 20771, USA
Anand.K.Bhatia@nasa.gov

Abstract. In previous papers (Sinha and Bhatia, *Phys. Rev. A* **83**, 063417 (2011), and Bhatia and Sinha, *Phys. Rev. A* **86**, 053421 (2012)) cross sections for the free-free transitions are calculated for a low energy (external) electron hydrogen scattering in the presence of an external homogeneous, monochromatic, and linearly polarized laser field, without and with the presence of plasma screening, respectively. The present calculation is extended to hydrogenic systems with nuclear charge greater than one. The Debye-Hückel approximation is used to investigate the effect of plasma screening. Calculations are carried out in the soft photon limit. The incident electron is considered to be dressed by the laser field non-perturbatively by choosing the Volkov solutions in both the initial and final states. The scattering wave function for the electron is obtained in the exchange approximation. The laser-assisted differential and total cross sections are calculated for single photon emission or absorption and no photon-exchange in the soft-photon limit, the laser intensity being much less than the atomic field intensity. The calculations have been carried out for various values of Debye parameter μ, ranging from 0.08 to 0.30. A strong suppression is noted for the laser-assisted singlet and triplet cross sections compared to the field-free situation. The suppression depends on μ, state of the system as well as on the incident electron momentum. This is unlike in the case of the hydrogen atom in the laser field where the suppression was much more for the triplet cross sections compared to the field-free situation.

Keywords. Electron or positron scattering; Atomic and molecular hydrogen targets; Eikonal-Born-series; Scattering cross sections; Screening by plasma; Debye screening length

PACS. 34.80.Qb; 34.50.Rk

Received: June 16, 2015 **Accepted:** June 28, 2015

1. Introduction

Among the many papers published on the scattering of radiation fields by free electrons is the pioneering work of Sen Gupta [1] and Vachaspati [2]. Since the invention of lasers in 1960, various types of lasers (atomic, molecular, gaseous, ion, semiconductor, solid state etc.) have become available. The laser can be continuous wave (cw), single mode type or high intensity, ultrashort pulse type. They have become an important tool for the study of atomic and molecular spectroscopy and of optical interactions with matter. The spectral output of lasers ranges from X-ray to far infra-red regions, having spectral widths as narrow as 20 Hz. There are number of applications of lasers in physical processes, such as isotope separation, gas breakdown, laser-induced fusion achieved by blasting tiny hydrogen pallets by laser pulses, optical tweezers invented to control the motion of matter [3]. These tweezers have been used to study Brownian motion [4]. CO_2 lasers have industrial applications (fiber optics, telecommunications etc.) as well as medical applications. Most of the reaction and scattering processes are mainly laser-assisted or laser-induced processes. The laser-assisted processes (basic processes exist in the absence of the laser field) require much lower laser intensities than the laser-induced processes. Some nonlinear phenomena, not known ordinarily, have been observed in the laser-assisted collision processes, such as excitation, ionization, recombination, and free-free transition processes. For example, the character of the ionization process changes due to a tunneling mechanism in the presence of high-intensity and low-frequency lasers. A tightly bound electron can respond to the oscillating electric field of the laser, because the Coulomb attraction of the ion core combines with the laser electric field to form an oscillating barrier through which the electron can escape by tunneling [5]. The tunneled electron can return and either be scattered elastically or to re-ionize the residual system leading to nonsequential double ionization (NSDI) or nonsequential multiple ionization, it can recombine generating *high-harmonic generation* (HHG), and *high-order above-threshold ionization* (HATI). Therefore, further insight can be gained from laser-assisted collision experiments. Another application of lasers is cooling and trapping of atomic particles. Trapping of electrons and positrons has resulted in accurate measurements of the spin-flip frequency ν_S and the cyclotron frequency ν_C which are related by

$$\nu_S = \frac{1}{2} g \nu_C \,. \tag{1.1}$$

The factor g is not equal to 2 due to the quantum electrodynamic corrections and it is equal to $2(1 + \alpha/2\pi)$, where α is the fine-structure constant. The experimental determination of the ratio $g(e^-)/g(e^+)$ is found to be consistent with unity within ± 2 parts in 10^{12} [6].

The production of cold and trapped antihydrogen is an important topic in theoretical as well as in experimental physics. It is found that among all the processes, the most efficient process is three-body recombination using cold antiproton and positron plasma in the presence of a laser field. The excited state cross sections are enhanced in general at very low incident energies of positrons [7]. However, most of the cross sections are suppressed at higher energies. These studies, which are important to test the *CPT* invariance of the standard model of interactions between the fundamental particles as well as the gravitational equivalence principle between matter and antimatter, have also been carried out [7] in the presence of

Debye-Hückel potential [8]. In these calculations eikonal approximation has been used which may not be accurate at very low incident energies. At such energies, the short-range and long-range interactions must be included as shown in the e-H scattering calculations [9].

The interpretation of line emission from plasma requires knowledge of spectroscopic as well as collisional properties of the plasma constituents. Autoionization states are important in collision cross sections as well as in dielectronic recombinations. These states, formed by the interaction between the bound states and the adjacent continua, can be probed using multiphoton excitation [10]. Spin polarization of hydrogen atoms [11] has been measured by laser-induced fluorescence, produced via the photodissociation of thermal HBr molecules.

There is a transfer of energy from the laser field to plasma without altering its average properties. However, there can be a substantial narrowing of the spectral lines emitted from a plasma and their shapes can be altered due to decrease in the Stark broadening [11, 12, 12–14].

A number of calculations have been carried out on different atomic systems embedded in plasma as well as in laser field. In a recent publications [15], the effect of the laser field on the scattering cross sections of low-energy electrons incident on hydrogen atoms was investigated. It was found in this process, also known as radiative scattering, that all the cross sections were suppressed in the laser field. The suppression being different for the triplet and singlet cross sections compared to the laser-free cross sections (FF). Wallbank and Holmes [16] carried out experiments on the scattering of low-energy electrons from He atoms in the presence of a pulsed CO_2 laser. Our results for the H atom [15] were found to be in qualitative agreement with the experiment [16]. The calculation of [15] was further extended to the case when the system was also embedded in a plasma [17], because in most of experiments performed to study the interactions of electrons and positrons with atomic systems, the plasma environment is always present to some extent and it can significantly affect the interaction mechanism [17]. It should be noted that in these calculations [17] the low-energy incident electron is an external electron and not the plasma electron. The presence of the plasma, which weakens the Coulomb interactions between two charged particles, was simulated by using the Debye-Hückel potential [8]. The plasma affects the collision cross sections and it was found that in all cases the cross sections were suppressed as compared to FF cross sections.

As stated in [17, 18], although a plasma is often thought of as a quasineutral ensemble of electrons and completely stripped nuclei (such as protons), there is of course no such ideal plasma. First of all, 100% ionization is an asymptotic approximation, and second, there continuously exists with some orbiting electron ions that exhibit atomic bound state characteristics and undergo atomic processes. Most laboratory plasmas begin as a neutral atomic and molecular gas and they exist in various ionic states for a finite period of time until final degree of ionization is achieved. Therefore, we can assume that there are neutral hydrogenic atoms and hydrogenic ions in the plasmas which are surrounded by perturbing particles which produce a screened Coulomb potential.

2. Theory

The laser field is chosen to be homogeneous, monochromatic, and linearly polarized [15, 17], and is represented by $\vec{\varepsilon}(t) = \vec{\varepsilon}_0 \sin(\omega t + \varsigma)$, where ς is the initial phase of the laser field,

the corresponding vector potential in the dipole approximation is $\vec{A}(t) = \vec{A}_0 \cos(\omega t + \varsigma)$ with $\vec{A}_0 = c\vec{\varepsilon}_0/\omega$, we choose ς equal to zero in the present calculation. The laser field $\vec{\varepsilon}$ corresponds to laser polarization, parallel to the incident electron's momentum (parallel geometry). The present calculation is carried out for nuclear charge $Z = 2$ to 10, $Z = 1$ results having been discussed in [17]. The energy of the laser field is $\omega = 0.0043$ a.u. $= 0.117$ eV (1 a.u. of energy being 219474.62 cm^{-1}), i.e., we are dealing with soft photons and the strength of the laser field is $\varepsilon_0 = 0.01$ a.u. (1 a.u. being 5×10^9 V/cm). The incident energy k_i^2 of the electron ranges from 0.04 to 1 Ry or 0.544 to 13.605 eV in this calculation. The theory for the present calculation has already been given in [15, 17], therefore, we describe it briefly.

The free-free transitions in the presence of an external laser field is given by

$$\omega(l) + e^-(\vec{k}_i) + Tg(1s) \rightarrow e^-(\vec{k}_f) + Tg(1s). \tag{2.1}$$

The energy conservation for the above process is given by

$$k_f^2 = k_i^2 + 2l\omega, \quad l = 0, \pm 1, \tag{2.2}$$

where l is the number of photons absorbed or emitted. The processes in which $l > 0$ and $l < 0$ correspond to inverse Bremsstrauhlung (absorption) and stimulated Bremsstrauhlung (emission), respectively, while $l = 0$ corresponds to pure laser-assisted scattering; $\vec{k}_i$ and $\vec{k}_f$ are the incident and final momenta of the projectile electron and Tg in above equation represent any of the hydrogenic systems. The total Hamiltonian of the system in the laser field is given by

$$H = -(i\vec{\nabla}_1 + \vec{A})^2 - (i\vec{\nabla}_2 + \vec{A})^2 + V_D, \tag{2.3}$$

where V_D represents the Debye-Hückel potential [8] of the form

$$V_D = -\frac{2Z}{r_1} e^{-\mu r_1} - \frac{2Z}{r_2} e^{-\mu r_2} + \frac{2}{r_{12}} e^{-\mu r_{12}}, \tag{2.4}$$

where $\vec{r}_1$ and $\vec{r}_2$are the position vectors of the incident electron and the bound electron of the target ion, and r_{12} is the relative distance. The parameter μ is called the Debye screening parameter and is given by$\mu = \sqrt{4\pi n (Ze)^2/k_B T} = 1/D$, k_B is the Boltzmann constant, n is the plasma density which is the sum of electron and ion densities, and T is the temperature of the plasma. The Debye length is given by $D = 1/\mu$. Rydberg units are used throughout in this calculation. Therefore, μ has the units of $1/a_0$, where a_0 is the Bohr radius of the hydrogen atom and the cross sections are in units of a_0^2. We have carried out calculation for $\mu = 0.08$ to 0.30, which is a reasonable choice to study the effects on the scattering process in the presence of the Debye shielding [8]. For very low values of μ, it is very difficult to get converged results because then the system behaves like a Coulombic system and it is well known that differential cross sections for such systems diverge in the forward direction of scattering. For systems with $Z > 2$, we have restricted calculations for $\mu = 0.12$ and 0.30. The transition matrix for the laser-assisted process (1.1) is given by [17]

$$T_{if} = -i \int dt \langle \psi_f | V_f | \psi_i^+ \rangle, \tag{2.5}$$

where the perturbation is given by

$$V_f = \left(\frac{2Z}{r_1}e^{-\mu r_1} - \frac{2}{r_{12}}e^{-\mu r_{12}}\right). \tag{2.6}$$

The projectile electron is considered to be dressed by the laser field in a nonperturbative manner by choosing the Volkov solutions [19] in both the initial and final channels. The final channel asymptotic wave function in Eq. (2.5) satisfies the following Schrödinger equation:

$$\left[-(i\vec{\nabla}_1 + \vec{A})^2 - (i\vec{\nabla}_2)^2 - \frac{2Z}{r_2}e^{-\mu r_2} - E\right]\psi_f = 0. \tag{2.7}$$

In the present work, we have neglected the laser-target interactions as compared to the dominant projectile-target interactions at very low incident energies. Thus the final channel wave function is chosen as

$$\psi_f = \chi_{k_f}\phi_f\,. \tag{2.8}$$

The final state wave function ϕ_f is the same as the initial state wave function ϕ_0 and calculated in the presence of Debye-Hückel [8] potential. The time-dependent Schrödinger equation describing the wave function χ_k of the electron in the laser field in the Coulomb gauge is given by

$$i\frac{\partial\chi_k^C(\vec{r},t)}{\partial t} = [-\nabla^2 + H(t)]\chi_k^C(\vec{r},t). \tag{2.9}$$

The superscript "C" on the wave function $\chi_k^C(\vec{r},t)$ indicates the Coulomb gauge, $\vec{\nabla}\cdot\vec{A} = 0$ (also known as radiation gauge) and

$$H(t) = i\frac{2q}{c}\vec{A}(t)\cdot\vec{\nabla} + \frac{q^2}{c^2}A^2(t)\,. \tag{2.10}$$

In Eq. (2.10) $q = -e$ is the charge of the incident electron and the second term can be eliminated by a canonical transformation. The solution of Eq. (2.9) is given by the Volkov wave function [19]

$$\chi_k^C(\vec{r},t) = (2\pi)^{-3/2}\exp(i\vec{k}\cdot\vec{r} - i[E_k t - \vec{\alpha}_0\cdot\vec{k}\sin(\omega t - \delta)]), \tag{2.11}$$

where $E_k = k^2$ is the free energy and

$$\vec{A}(t) = \vec{A}_0\cos(\omega t - \delta), \quad \vec{\alpha}_0 = \vec{\varepsilon}_0/\omega^2. \tag{2.12}$$

Eq. (2.11) shows how the radiation field dresses the incident electron plane wave with virtual photons. Making use of the generating function of the Bessel functions [20], it was shown in [19] that Eq. (2.11) can be written as

$$\chi_k(r,t) = (2\pi)^{-3/2}\sum_{m=-\infty}^{\infty}(-i)^m J_m(k\alpha_0)\exp(i[\vec{k}\cdot\vec{r} - (E_k - m\omega)t]). \tag{2.13}$$

We have chosen δ equal to zero in Eq. (2.13) and the scattering function ψ_i^+ in the initial channel satisfies the three-body Schrödinger equation, obeying the incoming boundary condition:

$$(H-E)\psi_i^+ = 0. \tag{2.14}$$

The spatial part $\psi_s(\vec{r}_1,\vec{r}_2)$ of the scattering wave function ψ_i^+ is obtained numerically by calculating the scattering functions in the exchange approximation [21] for each required partial wave to obtain convergence of the cross sections. Finally, the transition matrix element for the laser assisted process is given by

$$T_{if} = \frac{-i}{(2\pi)^{1/2}} \sum \delta(E_{k_f} - E_{k_i} + l\omega) J_l(\vec{q}\cdot\vec{\alpha}_0) I\,, \tag{2.15}$$

where the summation is over l, $\vec{q} = \vec{k}_f - \vec{k}_i$ is the momentum transfer, and l is the number of photons absorbed or emitted. The space part of the transition matrix is given by

$$I = \iint d^3r_1 d^3r_2 \exp(i\vec{k}_f\cdot\vec{r}_1)\phi_0(\vec{r}_2) V_f(\vec{r}_1,\vec{r}_2)\psi_i^+(\vec{r}_1,\vec{r}_2). \tag{2.16}$$

The target dressing can be neglected in the weak field limit and then the laser-assisted *differential cross section* (DCS) for the elastic scattering, for l photons, can be related to the FF differential cross by the relation [17, 19]

$$\left[\partial\sigma^l(k_i,k_f(l))/d\Omega\right]_{\text{laser}} = [k_f(l)/k_i] J_l^2(\vec{q}\cdot\vec{\alpha}_0)[\partial\sigma/d\Omega]_{FF}, \tag{2.17}$$

where $[\partial\sigma/d\Omega]_{FF}$, which depends upon the charge of the nucleus, is the field-free elastic cross section, J_l are the Bessel functions of integer order l, as indicated earlier $\vec{q}$ is the momentum transfer, $\vec{k}_i$ and $\vec{k}_f$ are the initial and final momenta of the electron. The above relation is called Kroll-Watson [19] approximation which is formulated under the assumption that the laser-target interaction is negligible. The FF elastic differential and total cross section are calculated by calculating phase shifts in the exchange approximation [21]. *Total cross section* (TCS) is obtained by integrating over the angles.

The wave function $\psi_s(\vec{r}_1,\vec{r}_2)$ for the scattering in the exchange approximation [21] is given by

$$\psi_s(\vec{r}_1,\vec{r}_2) = u(\vec{r}_1)\phi_0(\vec{r}_2) \pm (1\leftrightarrow 2), \tag{2.18}$$

where

$$u(\vec{r}) = \frac{u(r)}{r} Y_{L0}(\Omega). \tag{2.19}$$

The upper sign (+) refers to the singlet states and the lower sign (-) to the triplet states. The ground state wave function of the target in the presence of the Debye-Hückel potential [8] is given by ϕ_0(cf. Appendix). The equation for the scattering function *u(r)* is obtained from

$$\langle Y_{L0}(\Omega_1)\phi_0(\vec{r}_2)|H' - E|\psi_s(\vec{r}_1,\vec{r}_2)\rangle = 0. \tag{2.20}$$

The Hamiltonian in the above equation is given by

$$H' = -\nabla_1^2 - \nabla_2^2 + V_D. \tag{2.21}$$

Carrying out the integration gives the scattering equation for $u(r)$; by letting $r_1 = r$, we obtain

$$\left[\frac{d^2}{dr^2} - \frac{L(L+1)}{r^2} + \frac{2Z}{r}e^{-pr} - V_3(r) + k^2\right]u(r)$$
$$\pm\left\{r\phi_0(r)\delta_{Lo}F_1 - \frac{2}{(2L+1)}\phi_0(r)x\left[\frac{e^{-\mu r}}{r^L}F(r) + r^{L+1}e^{\mu r}G(r)\right]\right\} = 0. \tag{2.22}$$

The various quantities are given in [17]. Because of the parameter μ, the resulting integro differential is quite different from the well-known exchange approximation equation [21]. As explained in [17], the long-range polarization potential arising from the expansion of $1/r_{12}$ does not contribute in this problem because of the multiplying factor $e^{-\mu r_{12}}$ in the potential term $1/r_{12}$. Also, the inclusion of the short-range correlations [21] would be too much involved and they have not been included. At present, our main interest is to study the behavior of the elastic scattering (free-free) cross sections for various ions having nuclear charge greater than one in the combined effect of the laser field and the Debye-Hückel potential. We assume in the present work that beam penetration is not affected and the incident beam does not produce any penetration in the plasma. We have solved the resulting equation for the singlet and triplet states for the partial waves (L ranging from 0 to 49) for various values of μ by the noniterative method [22]. The phase shifts obtained have lower variational bounds and they are calculated from the function $u(r)$,

$$u(r) = A\sin\left(kr - \frac{L\pi}{2} + \eta\right) \quad \text{for } r \to \infty. \tag{2.23}$$

In spite of the fact that we are dealing with charged systems, the Coulomb phase has not been included in the above equation because the resulting field is no longer of the Coulomb form because of the presence of the term $e^{-\mu r}$ in the potential V_D. The FF elastic *differential cross section* (DCS) is given by

$$[d\sigma/d\Omega]_{FF} = (1/k_i^2)|\sum(2L+1)\exp(i\eta_L)\sin(\eta_L)P_L(\cos\theta)|^2, \tag{2.24}$$

where θ is the scattering angle between r and the z-axis and the summation is over L.

The momentum cross section is given by

$$\sigma(m) = \int(1-\cos(\theta))[\partial\sigma^l(k_i, k_f(l))/\partial\Omega]_{\text{laser}}d\Omega. \tag{2.25}$$

3. Results and Discussion

We have computed the *laser-assisted* (LA) differential and total cross sections for free-free transitions for the scattering of an electron from hydrogenic systems with the nuclear charge Z ranging from 2 to 10, embedded in a plasma and therefore the incident electron moves in a Debye-Hückel potential [8]. The laser polarization vector $\vec{\varepsilon}_0$ is parallel to the incident electron

momentum $\vec{k}_i$ ($\vec{\varepsilon}_0 \| \vec{k}_i$, parallel geometry), where $\vec{\varepsilon}_0$ is always along the polar axis. In Table 1, we show the convergence for the singlet and triplet (LA) total cross sections (TSC), along with the corresponding FF cross sections, with respect to the incident partial wave L. These TSC ($l = -1, 0$, and 1) and FF cross sections have been calculated at various incident momenta of the electron in the case of the three ions He^+, Li^{2+}, and Ne^{9+}. For high incident momentum k equal to 1.0, partial waves up to 49 are required to obtain convergence of the order of 1%. For lower values of k, fewer partial waves are required to obtain convergence of the order of 1%. These results are for the Debye parameter $\mu = 0.12$. We note that the LA cross sections are much lower than the FF cross sections.

The ion He^+ is much more amenable to experimental investigation, therefore, results for this ion are given in for singlet states in Tables 2, and for triplet states in Table 3, for various Debye parameter μ at various incident energies. We see, in the combined effect of the laser field and the Debye potential, the cross sections are very much suppressed as compared to the FF cross sections. The singlet cross sections, whether laser-assisted or FF, are lower than the triplet cross sections. The behavior of the LA cross sections is found to be opposite to that in the case of the neutral hydrogen atom embedded in a plasma [17]. It should be noted that it is not possible to compare the cross sections for the charged systems in the presence of the Debye potential with those in the absence of the Debye potential because the scattering cross sections are infinite for the charged systems. However, the presence of the Debye-Hückel potential reduces the cross sections even when the size of the system becomes larger as μ increases and at the same time the potential given in Eq. (2.6) becomes weaker as μ increases. It can be seen from Tables 2 and 3, where the calculations have been carried for He^+ ion for various values of μ. This is contrary to what was observed in the case of hydrogen [17] where the cross sections always increased when μ was increased and then started decreasing at higher values μ.

Figures 1-2 exhibit the effect of the laser field and plasma on the e-He^+ scattering cross sections. Figure 1 shows the behavior of total singlet cross section ($l = -1, 0$, and 1) at $k_i = 0.2$ with respect to μ, and similarly Figure 2 shows the behavior for the triplet states at $k_i = 0.2$. It is seen that the cross section is maximum for $l = 0$ in both cases.

Because of the presence of the nuclear charge Z in the potential given in Eq. (2.5), the cross sections are expected to increase as the nuclear charge is increased. We calculated TSC for $k_i = 0.2$ and 1.0 and for $\mu = 0.12$. We find LA singlet and triplet cross sections increasing as Z is increased from 2 to 10. These cross sections are exhibited in Figure 3 (triplet) and Figuer 4 (singlet) for $k_i = 1.0$ and for $\mu = 0.12$ for $Z = 2 - 10$. We see a continuous increase in both singlet and triplet TSC for $l = -1, 0$, and 1. We also carried out calculations at $\mu = 0.30$. A similar behavior is seen at $\mu = 0.30$. The results are given in Tables 4 and 5 for the singlet and triplet states, respectively. It seems that the cross sections continue to increase as Z increases. However, they are approximately proportional to Z^2 in spite of the presence of the repulsive-correlation potential between the electrons as indicated in Eq. (2.6). We can see the same behavior at other incident momenta as well.

In Table 6, $\sigma(m)$ is given for He^+ ion for various incident electron momenta and for $\mu = 0.2$ and for $l = -1, 0, 1$. They are small compared to the other laser-assisted cross sections given in various tables and $l = 0$ momentum cross sections are larger than those for $l = -1$ but smaller than those for $l = 1$.

Table 1. Convergence of the cross sections with respect to the angular momentum for various systems at various incident k for $\mu = 0.12$.

System	State	K	L_M^a	$l=-1$	$l=0$	$L=1$	FF
He^+	Singlet	0.8	25	25.431	146.804	89.370	692.863
			30	25.425	150.991	89.838	693.368
			35	25.399	152.932	89.979	693.521
		1.0	39	31.049	127.050	69.339	495.552
			44	30.217	127.879	68.670	495.559
			49	31.310	128.224	69.669	495.569
Li^{2+}		0.2	9	52.410	614.106	245.591	5251.151
			14	52.420	620.422	245.465	5251.981
			19	52.419	620.661	245.436	5251.983
		1.0	29	75.978	319.216	168.921	1223.163
			34	77.962	331.622	171.956	1225.618
			39	79.009	337.574	173.392	1226.333
			49	80.055	341.986	174.636	1226.740
Ne^{9+}		0.3	9	149.343	2597.376	452.773	12393.449
			14	150.074	2649.693	457.502	12412.457
			19	150.070	2651.598	457.071	12412.502
		1.0	39	293.936	1374.484	607.030	3962.852
			44	299.173	1396.724	613.896	3967.623
			49	301.768	1406.509	615.981	3968.982
He^+	Triplet	0.8	25	24.382	142.995	86.260	671.982
			30	24.377	147.163	86.730	672.487
			35	24.351	149.096	86.870	672.640
		1.0	39	30.666	125.506	68.463	494.322
			44	30.833	126.374	68.670	494.363
			49	30.925	126.717	68.791	494.373
Li^{2+}	Triplet	0.5	19	87.784	486.492	189.722	2396.137
			24	88.809	497.589	188.173	2397.325
			29	89.026	500.277	187.540	2397.424
		1.0	19	64.849	251.829	148.352	1190.593
			29	76.427	321.082	170.045	1226.460
			34	78.414	333.518	173.079	1228.916
			39	79.463	339.485	174.516	1229.630
			49	80.051	343.906	175.764	1230.038
Ne^{9+}		1.0	34	283.216	1324.457	588.322	3944.732
			39	293.620	1372.575	606.389	3961.079
			44	298.854	1394.795	613.250	3965.850
			49	301.446	1404.5722	615.331	3967.209

Table 2. Comparison of the singlet cross sections with FF cross sections for e-He^+ for various values of μ and k_i.

μ	k_i	$l=-1$	$l=0$	$l=1$	FF
0.08	0.2	6.858(1)	1.169(3)	2.587(2)	6.204(3)
	0.4	8.666(1)	9.067(2)	2.970(2)	3.407(3)
	0.6	8.920(1)	7.527(2)	2.381(2)	2.303(3)
	0.8	6.785(1)	5.436(2)	2.633(2)	1.573(3)
	1.0	9.470(1)	4.315(2)	2.048(2)	1.155(3)
0.10	0.2	4.123(1)	5.396(2)	1.817(2)	4.026(3)
	0.4	4.973(1)	4.274(2)	1.821(2)	2.184(3)
	0.6	5.425(1)	3.496(2)	1.544(2)	1.441(3)
	0.7	4.171(1)	2.876(2)	1.573(2)	1.201(3)
	0.8	4.005(1)	2.812(2)	1.486(2)	1.005(3)
	1.0	4.457(1)	1.768(2)	1.026(2)	7.126(2)
0.12	0.2	2.836(1)	3.059(2)	1.386(2)	2.928(3)
	0.4	3.297(1)	2.979(2)	1.142(2)	1.650(3)
	0.6	3.410(1)	1.897(2)	1.002(2)	9.976(2)
	0.8	2.540(1)	1.529(2)	8.998(1)	6.935(2)
	1.0	3.131(1)	1.282(2)	6.967(1)	4.956(2)
0.20	0.2	8.352	4.856(1)	4.147(1)	1.192(3)
	0.4	7.799	3.771(1)	2.951(1)	5.407(2)
	0.6	7.661	3.051(1)	2.271(1)	3.257(2)
	0.8	6.167	2.502(1)	1.904(1)	2.345(2)
	1.0	5.950	1.962(1)	1.350(1)	1.553(2)
0.30	0.2	1.717	9.582	8.641	2.665(2)
	0.4	1.778	6.824	6.192	1.875(2)
	0.6	1.621	5.319	4.545	1.068(2)
	0.8	1.593	5.086	4.373	8.662(1)
	1.0	1.272	3.540	2.769	5.579(1)

Table 3. Comparison of the triplet cross sections with FF cross sections for e-He^+ for various values of μ and k_i.

μ	k_i	$l=-1$	$l=0$	$l=1$	FF
0.08	0.2	6.851(1)	1.157(3)	2.604(2)	6.205(3)
	0.4	8.702(1)	9.102(2)	2.986(2)	3.415(3)
	0.6	8.855(1)	7.508(2)	2.359(2)	2.289(3)
	0.7	4.008(1)	2.809(2)	1.519(2)	1.167(3)
	0.8	3.816(1)	2.306(2)	1.373(2)	9.709(2)
	1.0	4.422(1)	1.756(2)	1.017(2)	7.099(2)
0.10	0.2	4.229(1)	5.524(2)	1.874(2)	4.082(3)
	0.4	4.969(1)	4.283(2)	1.819(2)	2.179(3)
	0.6	5.341(1)	3.458(2)	1.517(2)	1.427(3)
	0.7	4.008(1)	2.809(2)	1.519(2)	1.170(3)
	0.8	3.904(1)	2.781(2)	1.458(2)	9.834(2)
	1.0	4.422(1)	1.756(2)	1.017(2)	7.100(2)
0.12	0.2	2.811(1)	3.080(2)	1.355(2)	2.888(3)
	0.4	3.269(1)	2.964(1)	1.130(2)	1.640(3)
	0.6	3.338(1)	1.863(2)	9.784(1)	988.8(2)
	1.0	3.092(1)	1.267(2)	6.879(1)	4.944(2)
0.20	0.2	8.819	4.726(1)	4.249(1)	1.225(3)
	0.4	8.120	3.849(1)	3.045(1)	5.634(2)
	0.6	7.848	3.081(1)	2.309(1)	3.421(2)
	0.8	5.658	2.320(1)	1.752(1)	2.315(2)
	1.0	5.957	1.960(1)	1.350(1)	1.584)2)
0.30	0.2	3.238	1.749(1)	1.674(1)	3.682(2)
	0.4	2.166	8.261	7.583	1.970(2)
	0.6	1.927	6.175	5.342	1.196(2)
	0.8	1.505	4.759	4.092	9.697(1)
	1.0	1.324	3.665	2.876	5.822(1)

Table 4. Comparison of the singlet cross sections with FF for various systems, $\mu = 0.12$, and 0.30.

System	μ	K	$l = -1$	$l = 0$	$l = 1$	FF
Li^{2+}	0.12	0.2	5.242(1)	6.207(2)	2.454(2)	5.252(3)
		0.5	8.583(1)	4.672(2)	1.922(2)	2.356(3)
		0.8	5.671(1)	3.798(2)	2.085(2)	1.535(3)
		1.0	8.006(1)	3.420(2)	1.746(2)	1.226(3)
	0.30	1.0	5.321	1.511(1)	1.164(1)	2.068(2)
Be^{3+}	0.12	0.2	7.067(1)	8.437(2)	3.255(2)	6.657(3)
		1.0	1.239(2)	5.434(2)	2.670(2)	1.823(3)
	0.30	1.0	7.391	2.231(1)	1.653(1)	2.804(2)
B^{4+}	0.12	0.2	1.080(2)	1.670(3)	3.804(2)	8.897(3)
		1.0	1.600(2)	7.183(2)	3.401(2)	2.287(3)
	0.30	1.0	1.111(1)	3.398(1)	2.501(1)	3.864(2)
C^{5+}	0.12	0.2	4.801(1)	8.841(2)	1.474(2)	4.333(3)
		1.0	1.932(2)	8.761(2)	4.067(2)	2.708(3)
	0.30	1.0	1.265(1)	3.958(1)	2.853(1)	4.456(2)
N^{6+}	0.12	0.2	5.254(1)	6.388(2)	2.239(2)	6.051(3)
		1.0	2.233(2)	1.026(3)	4.652(2)	3.064(3)
	0.30	1.0	1.498(1)	4.825(1)	3.418(1)	4.998(2)
O^{7+}	0.12	0.2	1.117(2)	1.792(3)	3.699(2)	9.692(3)
		1.0	2.510(2)	1.158(3)	5.192(2)	3.396(3)
	0.30	1.0	1.767(1)	5.717(1)	4.030(1)	5.730(2)
F^{8+}	0.12	0.2	5.833(1)	1.049(3)	1.773(2)	6.869(3)
		1.0	2.759(2)	1,283(3)	5.657(2)	3.678(3)
	0.30	1.0	1.833(1)	6.036(1)	4.183(1)	6.035(2)
Ne^{9+}	0.12	0.2	1.501(2)	2.651(3)	4.573(2)	1.241(4)
		1.0	3.018(2)	1.407(2)	6.160(2)	3.969(3)
	0.30	1.0	2.035(1)	6.832(1)	4.676(1)	6.457(2)

Table 5. Comparison of the triplet cross sections with FF for various systems, $\mu = 0.12$, and 0.30.

System	μ	K	$l = -1$	$l = 0$	$l = 1$	FF
Li^{+2}	0.12	0.2	4.815(1)	5.272(2)	2.393(2)	4.706(3)
		0.5	8.903(1)	5.003(2)	1.875(2)	2.397(3)
		0.8	5.727(1)	3.906(2)	2.112(2)	1.548(3)
		1.0	8.005(1)	3.439(2)	1.758(2)	1.230(3)
	0.30	1.0	5.113	1.456(1)	1.119(1)	2.032(2)
Be^{3+}	0.12	0.2	7.201(1)	8.602(2)	3.315(2)	6.716(3)
		1.0	1.233(2)	5.411(2)	2.656(2)	1.818(3)
	0.30	1.0	7.851	2.355(1)	1.755(1)	2.909(2)
B^{4+}	0.12	0.2	1.080(2)	1.670(3)	3.804(2)	8.897(3)
		1.0	1.602(2)	7.180(2)	3.409(2)	2.294(3)
	0.30	1.0	1.104(1)	3.666(1)	2.479(1)	3.882(2)
C^{5+}	0.12	0.2	4.651(1)	8.676(2)	1.387(2)	4.209(3)
		1.0	1.927(2)	8.739(2)	4.053(2)	2.703(3)
N^{6+}	0.12	0.2	5.255(1)	6.382(2)	2.228(2)	6.050(3)
		1.0	2.239(2)	1.028(3)	4.665(2)	3.069(3)
	0.30	1.0	1.526(1)	4.904(1)	3.480(1)	5.046(2)
O^{7+}	0.12	0.2	1.086(2)	1.727(3)	3.486(2)	9.514(3)
		1.0	2.505(2)	1.155(3)	5.180(2)	3.392(3)
	0.30	1.0	1.754(1)	5.669(1)	3.996(1)	5.726(2)
F^{8+}	0.12	0.2	5.883(1)	1.048(3)	1.810(2)	6.888(3)
		1.0	2.764(2)	1.285(3)	5.668(2)	3.682(3)
	0.30	1.0	1.818(1)	6.001(1)	4.152(1)	5.996(2)
Ne^{9+}	0.12	0.2	1.501(1)	2.662(3)	4.558(2)	1.241(4)
		1.0	3.014(2)	1.405(3)	6.153(2)	3.967(3)
	0.30	1.0	2.056(1)	6.899(1)	4.726(1)	6.484(2)

Table 6. Momentum transfer cross section (a_0^3) for various k and $\mu = 0.2$.

k	State	$l=-1$	$l=0$	$l=1$
0.2	singlet	2.414	3.497	6.025
0.4		5.637(-1)	7.969(-1)	1.213
0.6		2.282(-1)	3.204(-1)	4.532(-1)
0.8		1.226(-1)	1.710(-1)	2.234(-1)
1.0		6.631(-2)	9.269(-2)	1.131(-1)
0.2	triplet	2.449	3.595	6.265
0.4		5.883(-1)	8.304(-1)	1.265
0.6		2.420(-1)	3.365(-1)	4.731(-1)
0.8		1.230(-1)	1.675(-1)	2.148(-1)
1.0		6.681(-2)	9.454(-2)	1.151(1)

Table 7. Ground state energies E_0 (Ry) of hydrogenic systems for various values of μ.

System	$\mu = 0.12$	$\mu = 0.30$
He^+	−3.540800	−2.923686
Li^{2+}	−8.301053	−7.327045
Be^{3+}	−15.06118	−13.72886
B^{4+}	−23.82127	−22.30421
C^{5+}	−34.58132	−32.53078
N^{6+}	−47.34136	−44.93135
O^{7+}	−62.10139	−59.33179
F^{8+}	−78.86141	−75.73213
Ne^{9+}	−97.62143	−94.13241

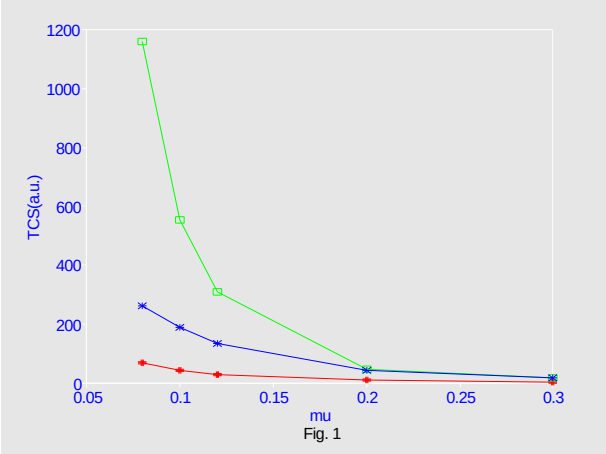

Figure 1. (Color online) Total cross sections (TCS) vs $\mu = 1D$ in a.u. for triplet state $k_i = 0.2$ for e-He^+ ion. The upper curve is for ($l = 0$), the middle curve is for single photon absorption ($l = 1$), and the lowest one is for emission ($l = -1$).

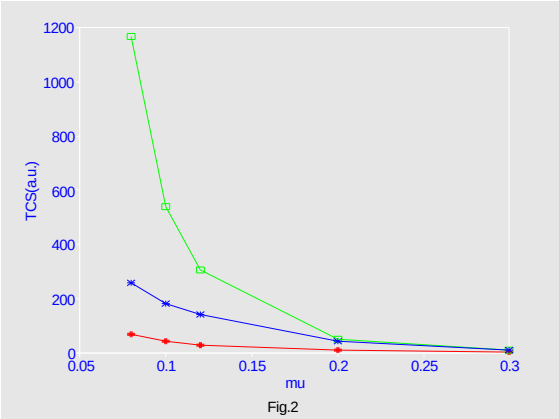

Figure 2. (Color online) Total cross sections (TCS) vs $\mu = 1/D$ in a.u. for singlet state $k_i = 0.2$ for e-He^+ ion. The upper curve is for ($l = 0$), the middle curve is for single photon absorption ($l = 1$), and the lowest one is for emission ($l = -1$).

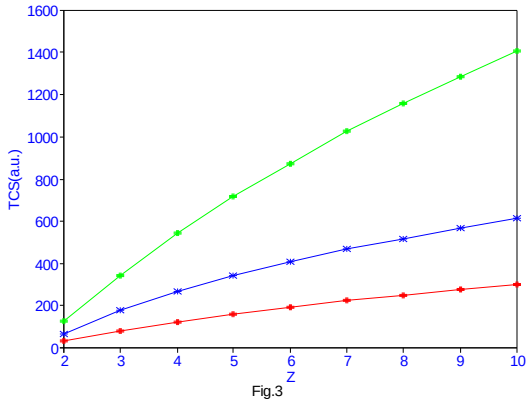

Figure 3. (Color online) Total cross sections (TCS) vs Z, the nuclear charge, for $\mu = 1/D = 0.12$ in a.u. for triplet state for $k_i = 1.0$. The upper curve is for ($l = 0$), the middle curve is for single photon absorption ($l = 1$), and the lowest one is for emission ($l = -1$).

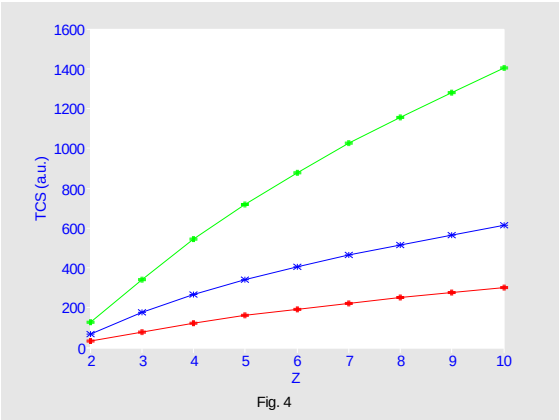

Figure 4. (Color Online) Total cross sections (TCS) vs Z, the nuclear charge, for $\mu = 1/D = 0.12$ in a.u. for singlet state for $k_i = 1.0$. The upper curve is for ($l = 0$), the middle curve is for single photon absorption ($l = 1$), and the lowest one is for emission ($l = -1$).

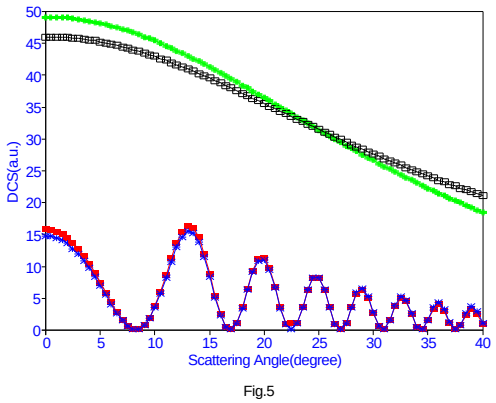

Figure 5. (Color Online) Singlet and triplet DCS for $k_i = 0.2$, $\mu = 0.2$ and $l = -1$ along with the corresponding FF DCS. The upper curves are singlet states for the scattering angles less than 25 degrees, then the lower curves are for singlet states. The FF DCS have been multiplied by a factor 0.1.

We present in Figure 5 some differential cross sections for both singlet and triplet along with their corresponding FF results for $k_i = 0.2$ and $\mu = 0.20$. The differential cross sections are given up to the scattering angle of 40 degrees. It is noticed that there is a strong modification (both quantitatively and qualitatively) in the laser assisted DCS as compared to the FF for both singlet and triplet states. The singlet DCS are higher than the triplet ones up to 24.5 degrees and after this the triplet DCS are higher. The oscillations shown in the figure are attributed to the oscillations of the Bessel functions occurring in the expression of DCS given in Eq. (2.17).

4. Conclusions

The presence of the Debye-Hückel potential ($\mu > 0$) suppresses the cross sections in all cases ($l = -1, 0$, and 1) and for all values of the incident momentum. This is opposite to the case of the hydrogen atom [17] in the laser field and the Debye-Hückel potential, where there was an enhancement for lower values ofμ. However, there is suppression of the field-free cross sections for all Z(1-10). The total cross section for absorption ($l > 0$) is always higher than that for emission ($l < 0$). A significant difference is noted in for the singlet and triplet states. The suppression is not always much more for triplet TSC as for $Z = 1$ [13]. The TCS increase as Z increases from 2 to 10. We have also calculated momentum cross sections for the He^+ ion for various values of incident momentum and these cross sections are small compared to all other cross sections. It is hoped that these cross sections could be measured. Such measurements would provide a further verification of the KWA approximation [19].

Appendix

As indicated in [17], the ground-state wave function of the hydrogenic systems gets dressed under the Debye-Hückel potential [8].

$$\phi_0 = e^{-ar} \sum_i C_i r^i \tag{A.1}$$

Since the lowest term does not have r, the summation index i ranges from 0 to $N = 14$, giving the maximum number of terms equal to 15. The corresponding energy is calculated variationally by using

$$\left\langle \phi_0 \left| -\nabla^2 - \frac{2Z}{r} e^{-\mu r} \right| \phi_0 \right\rangle = E_0 \phi_0 \,. \tag{A.2}$$

We find that the energy is not sensitive to the variation of the parameter a, therefore we keep it fixed equal to Z. Energies for various systems are given in Table 7 for $\mu = 0.12$ and 0.30. As μ increases, the ground-state energy decreases. The system becomes unbound for large values of μ.

Competing Interests

The author declare that they have no competing interests.

Authors' Contributions

The author contributed significantly in writing this article. The author read and approved the final manuscript.

References

[1] N. D. Sen Gupta, Bull. Math. Soc. Calcutta **41**, 187 (1949); ibid. **44**, 157 (1952).

[2] Vachaspati, Phys. Rev. **128**, 664 (1962).

[3] A. Ashkin, Phys. Rev. Lett. **24**, 156 (1970).

[4] T. Li et al., *Science* **328**, 1673 (2010).

[5] U. Eichmann, M. Dörr, H. Maeda, W. Becker, W. Sandner, Phys. Rev. Lett. **84**, 3350 (2000).

[6] R. S. Van Dyck Jr., P. B. Schwinberg, and H. G. Dehmelt, Phys. Rev. Lett. **50**, 26 (1987).

[7] S. Mukhopadhyay and C. Sinha, Phys. Rev. A **88**, 033414 (2013).

[8] P. Debye and E. Hückel, Phys. Z. **24**, 185 (1923).

[9] A. K. Bhatia, Phys. Rev. A **75**, 032713 (2007).

[10] J. H. Eberly, Phys. Rev. Lett. **47**, 408 (1981).

[11] L. Bougas, D. Sifikitis, M. A. Everest, A. J. Alexande, and T. P. Rakitzis, J. Chem. Phys. **133**, 174308 (2010).

[12] S. Alexiou, J. Quant. Spectrosc. Radiat. Transf. **71**, 139 (2001).

[13] S. Alexiou, P. Sauvan, A. Poquerusse, E. Leboucher-Dalimier, and R. W. Lee, Phys. Rev. E **59**, 3499 (1999).

[14] O. Blokhintsev, Phys. Z. Sowjetunion **4**, 601 (1933).

[15] C. Sinha and A. K. Bhatia, Phys. Rev. A **83**, 175201 (2010).

[16] B. Wallbank and J. K. Holmes, J. Phys. B **29**, 5881 (1996).

[17] A. K. Bhatia and C. Sinha, Phys. Rev. A **86**, 053421 (2012).

[18] *Methods of Experimental Physics*, Vol. 9, edited by H. R. Griem and R. H. Lovberg (Academic Press, New York), p.115.

[19] N. M. Kroll and K. M. Watson, Phys. Rev. A **8**, 804 (1973).

[20] G. N. Watson, *Theory of Bessel Functions*, 2^{nd} ed. (Cambridge University Press, Cambridge, 1962), p. 22.

[21] A. K. Bhatia, Phys. Rev. A **75**, 032713 (2007).

[22] K. Omidvar, Phys. Rev. **133**, A970 (1964).